Research Article

Synthesis and Characterization of Palm Oil-Based Polyurethane Reinforced with Surfactant-Modified Montmorillonite Nanoclay

Teuku Rihayat*, Suryani, Syafruddin, Muhammad Yunus and Satriananda
Department of Chemical Engineering, Politeknik Negeri Lhokseumawe, Aceh, Indonesia

Pocut Nurul Alam
Department of Chemical Engineering, Faculty of Engineering, Syiah Kuala University, Banda Aceh, Indonesia

Fanny Sakinah
Department of Chemical Engineering, Faculty of Engineering, Universitas Gajah Mada, Yogyakarta, Indonesia

* Corresponding author. E-mail: teukurihayat.1007@gmail.com DOI: 10.14416/j.asep.2026.05.006
Received: 17 October 2025; Revised: 8 December 2025; Accepted: 16 April 2026; Published online: 12 May 2026

Abstract
Polyurethane (PU) is a polymer with outstanding mechanical and elastic properties; however, most PUs are still derived from petrochemical-based polyols. This study aims to synthesize polyurethane from palm oil-based polyols obtained through esterification of oleic acid and glycerol using DBSA as a catalyst, and to reinforce it with montmorillonite (MMT) modified by surfactants (CTAB and ODA). FTIR and GPC analyses confirmed the successful formation of polyol (Mw ~950) and PU (Mw ~3266). XRD, SEM, and TEM results demonstrated well-dispersed intercalated–exfoliated structures within the PU matrix. Mechanical testing revealed more than a 200% improvement in tensile strength and elongation at break after organoclay incorporation, attributed to strong interfacial interactions between PU and MMT. DMA analysis indicated an increase in glass transition temperature (Tg), while TGA showed that the onset of degradation shifted from 200 °C for neat PU to ~318 °C for CTAB-mont-PU and ~330 °C for ODA-mont-PU. Overall, ODA-mont-PU exhibited the most significant improvements in morphology, mechanical performance, and thermal stability, highlighting its potential for advanced elastomer applications and as a sustainable alternative to petrochemical-based polyols. Unlike comprehensive reviews on construction-related nanotechnology, this work is an experimental study focusing on the synthesis of palm oil-based polyurethane and a head-to-head comparison of CTAB- and ODA-modified montmorillonite, supported by multi-technique characterization and kinetic degradation modeling.

Keywords: Nanocomposites, Organoclay, Palm oil-based polyol, Polyurethane (PU), Sustainable polymers

1 Introduction

Polyurethane (PUR) is a high-molecular-weight polymer formed by polyaddition of hydroxyl compounds and polyisocyanates with catalysts and additives. At present, most of the polyether polyols utilized in polyurethane production are sourced from petrochemical materials. These petrochemical feedstocks are derived from mineral oil, a non-renewable resource whose estimated reserves may only last for approximately the next fifty years, even under optimistic projections. Therefore, it is essential to explore and develop alternative renewable sources in the near future [1]. The development of biodegradable polymers from renewable resources is highly desirable for coating applications, as they can serve as sustainable alternatives to conventional paints while effectively protecting surfaces from microbial growth, physical degradation, and chemical reactions such as oxidation [2]. First synthesized by Otto Bayer in 1937 as a rubber substitute, PUR is now widely used in foams, elastomers, plastics, adhesives, coatings, and

leather-like materials. Its main raw materials are polyisocyanates, polyester or polyether polyols, chain extenders, and sometimes water or halohydrocarbons as blowing agents, flame retardants, and surfactants. Polyurethane elastomers (PUREs) exhibit high hardness, superior resistance to abrasion and chemicals, and outstanding mechanical and elastic characteristics, which can be customized by varying the composition of raw materials. Global PUR production grew rapidly, reaching 8,821 billion tonnes by 2005, ranking fifth after major plastics.

Bentonite is an economical filler mineral primarily composed of montmorillonite ($Al_2O_3{\cdot}4SiO_2{\cdot}xH_2O$). It is abundant in Indonesia and consists of fine phyllosilicate particles (<2 μm) containing silica, alumina, and hydroxides. Structurally, bentonite has a layered arrangement of two tetrahedral silica sheets and one central octahedral sheet [3]. To improve performance, PUR/clay nanocomposites using palm-oil-based polyols have been developed, yielding higher modulus, strength, and heat resistance. PUREs, composed of soft polymer-glycol and hard diisocyanate segments, provide superior resilience, load-bearing capacity, and resistance to aging, ozone, solvents, and oils [4]. PUR properties can be enhanced by modifying its building blocks or adding inorganic fillers such as calcium carbonate, aluminum hydroxide, kaolin, titanium, zinc oxide, or silica to improve stiffness, barrier properties, and fire resistance, or to reduce cost [5]. This study combines both approaches using palm-oil polyol and layered silicate (clay).

Most industrial polyols remain petrochemical-based, but renewable oils such as palm kernel, vernonia, castor, and cardanol have been explored as sustainable alternatives, with Malaysia leading research on palm-oil polyols [6]. In 1995, Malaysia and Indonesia dominated global palm-oil exports, producing 6.54 and 2.37 million tonnes respectively [7]. Natural oils are abundant, low-cost feedstocks suitable for polymer production [8], [9]. Clay minerals, especially 2:1 phyllosilicates, provide layered structures with cation-exchange capacity that strengthen nanocomposites [10]. The structural arrangement of 2:1 phyllosilicate layers is illustrated in Figure 1, where tetrahedral sheets sandwich an octahedral sheet, creating interlayer spaces that contain exchangeable cations.

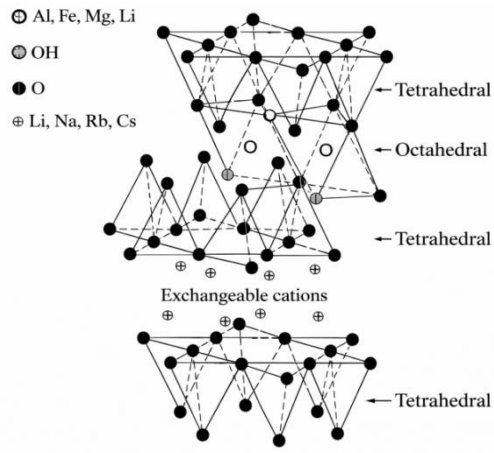

Figure 1: Structure of 2:1 phyllosilicates.

The layered silicates most frequently employed in polymer–clay nanocomposites include montmorillonite (MMT), hectorite, and saponite. Layered silicates can be tetrahedrally or octahedrally substituted, with tetrahedral substitution providing surface charges that promote stronger interaction with polymer matrices [11]. Their key features are the ability to disperse into individual layers and the tunable surface chemistry achieved by ion exchange with various cations, both of which control dispersion in polymers [12]. Polymer–clay nanocomposites have drawn strong industrial and academic interest for their superior properties over pure polymers or conventional composites, first reported by Blumstein in 1961 and later advanced by Toyota researchers in 1988 [13]. Modern methods incorporate modified silicates into polymers via in situ polymerization, solvent-swelling, or melt blending [14]. Since Usuki's 1993 studies, nanocomposites have been developed with polymers such as poly(ε-caprolactone), polystyrene, epoxy, and polyimide, as well as polyurethane (PU) [15].

Petroleum-based PU/clay nanocomposites show improved mechanical, thermal, and water-resistance properties compared with pure PU, but studies using palm-oil-based polyol remain limited. This study aims to synthesize polyurethane using palm-oil-based polyol, incorporate various organophilic clays, and evaluate the resulting PU/clay nanocomposites. Characterization includes XRD, FTIR, GPC, DMA, tensile testing, SEM/TEM, and TGA to assess mechanical, thermal, and morphological properties, with a focus on partially replacing petrochemical polyols and reinforcing PU with montmorillonite.

The use of palm-oil-based polyols represents a strategic approach toward sustainable materials development. As a renewable and abundant feedstock, palm oil reduces reliance on petrochemical polyols derived from non-renewable fossil resources. The incorporation of biobased polyols helps to lower the carbon footprint of polyurethane production, supports circular bioeconomy initiatives, and aligns with global efforts to transition toward environmentally responsible polymeric materials. In this context, palm-oil-derived polyols offer a promising pathway for producing high-value polyurethane materials while enhancing the overall sustainability of the polymer supply chain.

Compared with previous studies on polyurethane/montmorillonite (PU/MMT) nanocomposites, this work provides several key novelties. First, palm-oil-based polyols synthesized via DBSA-assisted esterification were combined with two different surfactant-modified clays, namely CTAB-MMT and ODA-MMT, allowing a comparative evaluation of their effects on dispersion and interfacial interactions. Second, a comprehensive multi-technique characterization approach was performed, including FTIR, GPC, XRD, TEM, SEM, DMA, TGA kinetic analysis, and mechanical performance modeling, which has not been simultaneously reported in earlier studies. Third, a pseudo–first-order kinetic model was applied to quantify the improvement in thermal stability, providing a deeper understanding of degradation mechanisms. These contributions establish the scientific novelty and added value of the present research.

2 Material and Methods

2.1 *Materials*

The main materials used include Kunipia-F (Na+ montmorillonite), 4,4-diphenylmethane diisocyanate (MDI), palm oil–based polyol, glycerol, oleic acid, and 4-dodecylbenzenesulfonic acid (DBSA) as emulsifier-catalyst. Other reagents are 1,4-butanediol (BDO) as a chain extender, cetyltrimethyl ammonium bromide (CTAB) and octadecylamine (ODA) for clay modification, as well as solvents such as dimethylformamide (DMF), ethanol, and dioxane. All reagents were of analytical grade and were used without further purification.

2.2 *Methodology*

This research involves the preparation and characterization of palm oil–based polyol, the synthesis of polyurethane (PU) from this renewable source, the modification of montmorillonite into organophilic clay, and the development of PU/clay nanocomposites. The objective is to produce environmentally friendly polyurethane composites with improved mechanical, thermal, and morphological properties by combining renewable palm oil polyol with modified clays as reinforcing agents.

2.2.1 Synthesis of palm oil polyol

Palm oil–based polyol was synthesized through the esterification of oleic acid and glycerol using a three-necked flask fitted with a mechanical stirrer and a cooling apparatus. DBSA served as both emulsifier and catalyst, promoting homogeneous mixing of the immiscible reactants. After the reaction, the product was filtered to remove molecular sieves and washed with sodium chloride solution to eliminate excess glycerol. The overall synthesis pathway of polyurethane derived from palm oil polyol is illustrated in Figure 2.

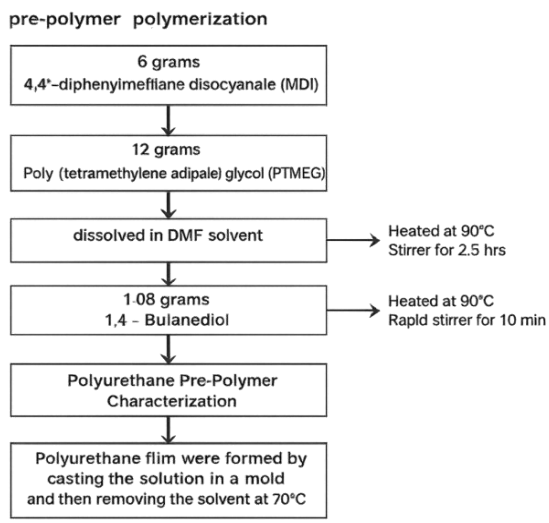

Figure 2: Synthesis of polyurethane

The esterification route was selected as the primary method for polyol preparation due to the high reactivity of oleic acid toward glycerol in the presence

of a sulfonic acid catalyst. In this work, the reaction was conducted at 180–200 °C with an oleic acid:glycerol molar ratio of 1:3 to ensure sufficient hydroxyl functionality. DBSA was used at 1 wt% as both emulsifier and catalyst, promoting homogeneous mixing of the immiscible reactants. The reaction time (4–6 h) was optimized to achieve complete conversion while avoiding thermal degradation. Optimization was guided by monitoring the hydroxyl number (OH value), acid number, and viscosity of the resulting product. The final polyol exhibited an OH number suitable for polyurethane synthesis, confirming the successful formation of palm-oil-based polyol.

2.2.2 Preparation of Thermoplastic Polyurethane (TPU)

The polyurethane prepolymer was synthesized by reacting palm oil polyol with MDI at 70–80 °C under nitrogen at a specific NCO/OH ratio. To clarify the formulation, the NCO/OH ratio used in this work was 1.05, corresponding to a 5% excess of isocyanate groups. This ratio was selected to ensure complete conversion of hydroxyl groups while minimizing unreacted NCO at the end of the prepolymer step. The amount of 1,4-butanediol (BDO) chain extender was calculated based on the remaining NCO groups to achieve a 1:1 stoichiometric balance between the residual NCO and the OH groups of BDO during the chain-extension reaction. The use of an NCO/OH ratio slightly above unity is known to increase crosslink density and produce polyurethane with enhanced stiffness, modulus, and tensile strength compared to formulations with an exact 1.0 ratio.

The reaction progress was monitored using FTIR to determine the isocyanate content. After reaching the theoretical NCO percentage, the prepolymer was cooled and stored. In the second step, the prepolymer was chain-extended with 1,4-BDO at 90–100 °C to form TPU films, which were cast in molds and dried under pressure at 70 °C.

2.2.3 Preparation of organophilic clay

Kunipia-F montmorillonite was modified with CTAB or ODA to enhance compatibility with the polyurethane matrix. CTAB was dissolved in distilled water at 80 °C and mixed with a dispersed Kunipia-F suspension. The mixture was stirred for 1 hour, washed repeatedly to remove residual salts, and oven-dried at 60 °C. The dried organoclay was ground and sieved to obtain particles smaller than 100 μm.

2.2.4 Preparation of PU/Clay nanocomposites

Polyurethane/clay nanocomposites were produced by melt blending PU with 1–5 wt% organoclay using a Haake internal mixer at 80 °C and 50 rpm. The blends were then compression-molded at 100 °C into 1 mm sheets for subsequent analysis. Both CTAB- and ODA-modified clays were used to investigate the effect of different surfactant treatments on the composite properties.

2.2.5 Characterization techniques

The synthesized materials were comprehensively characterized using a range of analytical techniques. Gel permeation chromatography (GPC) and Fourier transform infrared spectroscopy (FTIR) were employed to determine the molecular weight of the polyols, identify functional groups, and confirm polyurethane formation. X-ray diffraction (XRD), scanning electron microscopy (SEM), and transmission electron microscopy (TEM) were used to evaluate the clay structure, dispersion, and morphology within the polyurethane (PU) matrix. Dynamic mechanical analysis (DMA) and tensile testing were conducted to assess mechanical properties and viscoelastic behavior. Additionally, thermogravimetric analysis (TGA) was performed to evaluate thermal stability and flame retardancy.

2.2.6 Modeling of mechanical properties

The reinforcement mechanism of nanoclay in the PU matrix was analyzed using Guth and Halpin–Tsai equations to model Young's modulus as a function of filler geometry and content.

3 Results and Discussions

This study involved synthesizing polyurethane (PU) from palm oil polyol, preparing clay nanocomposites with CTAB and ODA surfactants, and fabricating PU/clay composites. Characterization included TGA for thermal resistance, FTIR for micro-domain structures, tensile and DMA tests for mechanical properties, XRD for clay dispersion, and GPC for molecular weight analysis. The explanation has been revised to clarify that the mechanical reinforcement is predominantly governed by strong physical interactions—including Van der Waals forces, increased surface contact, and the physical

confinement effect of clay platelets—rather than the formation of new covalent bonds. Three main mechanisms contribute to the >200% improvement: (a) well-dispersed intercalated/exfoliated clay layers, which create a large interfacial area; (b) efficient stress transfer facilitated by strong hydrophobic interactions between ODA alkyl chains and the non-polar segments of PU; and (c) increased tortuosity for crack propagation due to the dispersed clay platelets, which absorb and dissipate energy. The Discussion section has been revised to emphasize the dominant role of physical confinement and effective shear stress transfer in enhancing the tensile properties of the PU/organoclay nanocomposites.

In terms of sustainability, the desirability of palm-oil-based polyurethane in this study refers specifically to the use of renewable feedstocks as a partial replacement for petrochemical polyols. However, a full quantification of environmental benefits—such as carbon footprint reduction, energy consumption, or overall life-cycle impact—requires a dedicated Life Cycle Assessment (LCA) study, which is beyond the scope of the present work.

3.1 *Synthesis of polyurethane based on palm oil*

Polyol The synthesis of polyurethane elastomers (PUEs) requires two groups of reactants: isocyanate groups and hydroxyl groups (polyols). In this work, palm oil was used as the raw material for producing polyol.

3.1.1 FTIR spectroscopy analysis

The functional group characterization of the polyol synthesized from oleic acid and glycerol is presented in Figure 3. A broad absorption peak at 3384 cm^{-1} confirms the presence of hydroxyl groups (–OH), which serve as the active sites for subsequent polymerization. The long-chain hydrocarbon backbone of the fatty acid is identified by the sharp sp^3 C–H stretching vibration at 2926 cm^{-1}. The appearance of a strong peak at 1741 cm^{-1} indicates the formation of ester linkages (C=O) resulting from the esterification reaction between the carboxyl groups of oleic acid and glycerol [16]. Furthermore, peaks at 1174 cm^{-1} and 1039 cm^{-1} correspond to C–O–C and C–O stretching vibrations, respectively, providing further evidence of the polyol ester structure.

The synthesis of polyurethane (PU) was monitored periodically via FTIR spectra, as shown in Figure 4. The most significant change is observed in the 2270 cm^{-1} region, which is the characteristic absorption of the isocyanate group (–N=C=O). As the reaction progressed from 0 to 7 hours, the intensity of this peak decreased drastically and completely disappeared by the 7th hour. This indicates that all the isocyanate groups had fully reacted with the –OH groups of the polyol.

The successful formation of urethane linkages is confirmed by the emergence of new absorption bands at 3320 cm^{-1} (N–H stretching) and the amide I region between 1700–1730 cm^{-1}. The peak at 1709 cm^{-1} indicates the presence of hydrogen-bonded carbonyl groups (bonded C=O), while the shoulder at 1731 cm^{-1} represents free carbonyl groups (free C=O) [17]. Additionally, the N–H bending vibration appearing around 1530 cm^{-1} collectively proves the transition from monomeric precursors to a stable polyurethane polymer network.

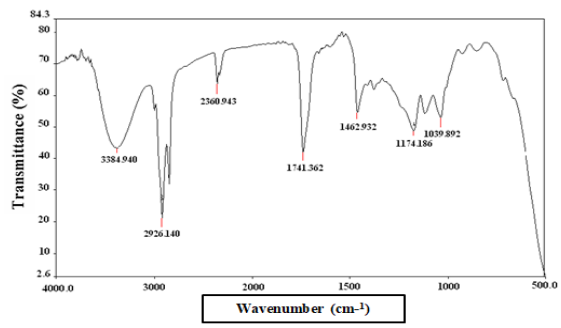

Figure 3: The FTIR spectra of the synthesized polyol based on palm oil.

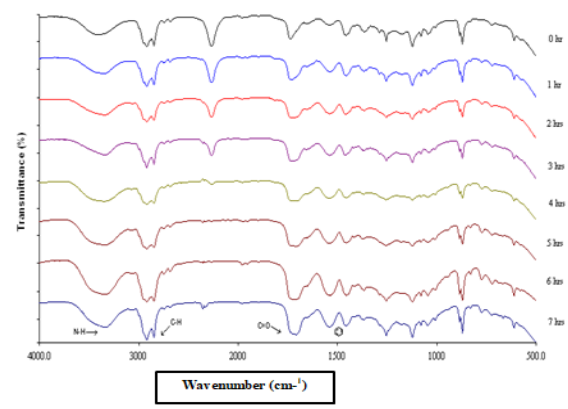

Figure 4: The FTIR spectra of the synthesized polyurethane based on palm oil polyol.

3.1.2 Molecular weight

GPC/SEC analysis showed palm-oil polyol with Mw = 955, Mn = 679, Mz = 1256, Đ = 1.4 (Figure 5 and 6). After PU synthesis, molecular weights increased markedly (Mw = 3266, Mn = 1425, Mz = 10090, Đ = 2.29), confirming high polymer formation. Molecular weight fractions influence mechanical behavior, where Mn relates to brittleness/flow, Mw to strength/impact resistance, and Mz to flexibility. PU consists of soft segments (polyol) providing elasticity and hard segments (isocyanates) providing rigidity and hydrogen bonding [18], [19].

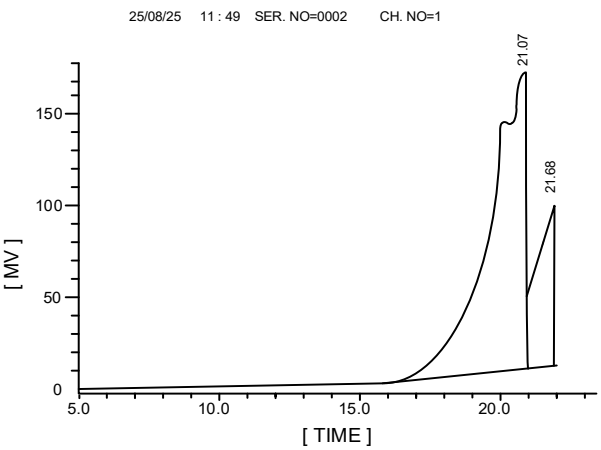

Figure 5: The GPC profiles of the polyol based on palm oil.

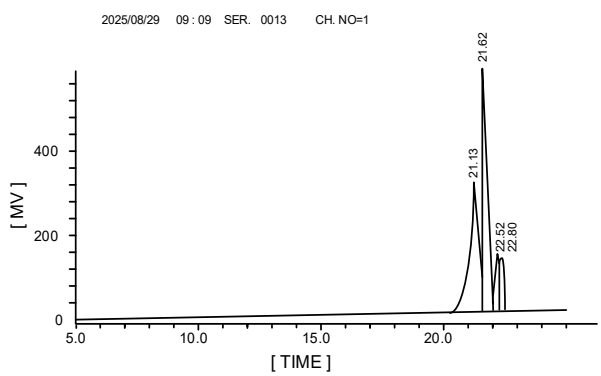

Figure 6: The GPC profiles of the synthesized polyurethane based on palm oil polyol

In polyurethane elastomers, soft segments govern elasticity, extensibility, and low-temperature performance, while hard segments control modulus, tear strength, and tensile properties. Crystallinity, melting point, and strain-induced crystallization further influence performance, with diisocyanate structure enhancing hydrogen bonding and network strength [20], [21].

3.2 *Preparation of organoclay nanocomposites using different surfactants (CTAB and ODA)*

Polyurethanes (PUs) possess good abrasion resistance, tear strength, flexibility, and elasticity but limited thermal stability. This can be improved by adding <10 wt.% modified montmorillonite (MMT), which enhances both thermal and mechanical properties [22]. Ion exchange with alkylammonium cations converts hydrophilic MMT into organophilic clay with expanded galleries.

This interlayer expansion is clearly evidenced by the shift of the diffraction peaks toward lower 2θ angles in the WAXD patterns Figure 7. The characteristic peak of pure-mont at 7.78° significantly shifted to 5.72° for CTAB-mont and 5.316° for ODA-mont. These shifts correspond to an increase in basal spacing (d-spacing) from 1.142 nm (pure MMT) to 1.571 nm (CTAB-modified) and 1.798 nm (ODA-modified), respectively.

The greater expansion observed for ODA-modified MMT suggests that the longer alkyl chain of octadecylamine (ODA) provides more effective steric hindrance and packing within the silicate galleries compared to cetyltrimethylammonium bromide (CTAB). This expansion confirms the successful intercalation of alkylammonium cations, which reduces the surface energy of the clay and enhances its compatibility with the hydrophobic polyurethane matrix. The enlarged gallery spacing also facilitates the diffusion of polyurethane chains into the interlayer regions during nanocomposite formation, leading to improved dispersion of clay platelets and enhanced overall material performance.

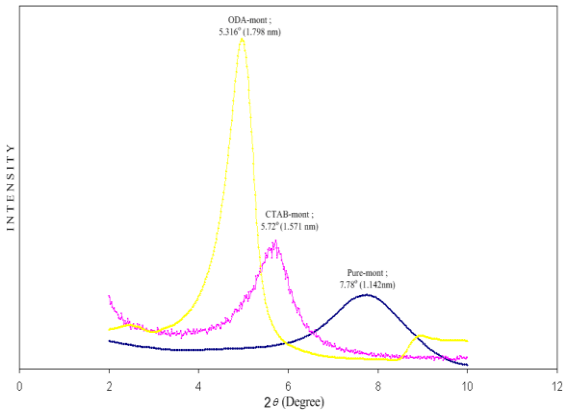

Figure 7: The WAXD pattern of pure-PU.

Furthermore, the broadening of the peaks in the modified MMT samples compared to the relatively sharper peak of pure MMT suggests a slight reduction in the long-range crystalline order of the clay stacks after surfactant intercalation. This phenomenon occurs because the insertion of bulky organic cations such as ODA and CTAB disrupts the original periodic arrangement of the clay layers. The significantly lower 2θ value observed for ODA-modified MMT indicates a more extensive gallery expansion, suggesting that the long-chain ODA molecules may adopt a more ordered paraffin-type arrangement within the galleries. Such structural modification plays a crucial role in determining the efficiency of polymer chain diffusion into the clay layers and ultimately influences the morphology and performance of the resulting polyurethane/clay nanocomposites.

3.3 *Synthesis of palm oil–based polyurethane matrix reinforced with clay nanocomposites*

3.3.1 WAXD curves

Sodium-type montmorillonite (Na^+-MMT) has negatively charged silicate layers with sodium ions, dispersing well in water but not in polymers due to high hydrophilicity. By exchanging sodium with organic cations, it becomes organophilic, reducing hydrophilicity and allowing better dispersion in polymer matrices (Figure 8).

Figures 9 and 10 show the WAXD curves of PU/clay nanocomposites prepared with CTAB- and ODA-modified montmorillonite. In both cases (CTAB-mont-PU and ODA-mont-PU), clear diffraction peaks were observed in the range of 2θ = 2–10° for composites containing 1, 3, and 5% clay. These results confirm that the organoclays were successfully intercalated within the polyurethane matrix.

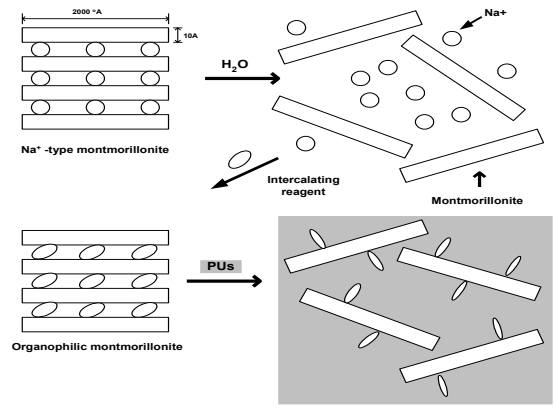

Figure 8: Dispersive behavior of montmorillonite.

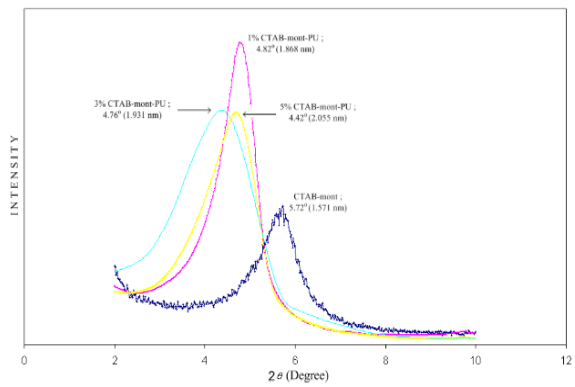

Figure 9: WAXD pattern of CTAB–mont–PU nanocomposite.

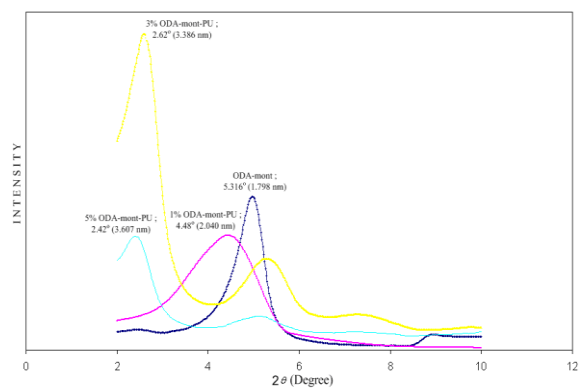

Figure 10: WAXD pattern of ODA-mont-PU nanoocomposite.

In 1% CTAB-mont-PU, a small peak at 2θ = 4.82° (d = 1.868 nm) was observed, with spacing increasing to 2.055 nm at 5% loading. ODA-mont-PU showed larger interlayer spacings than CTAB-mont-PU, due to the bigger molecular size of octadecylamine compared to cetyltrimethyl ammonium bromide [23]. Detailed values are given in Table 1.

Table 1: Summary of d-spacing (nm) and 2θ (°) values for Pure Kunipia, CTAB–mont, ODA–mont, CTAB–mont–PU, and ODA–mont–PU samples.

Materials	2 θ (degree)	*d*-spacing (nm)
Kunipia	7.78	1.142
CTAB-mont	5.72	1.571
ODA-mont	5.31	1.798
1% CTAB-mont-PU	4.82	1.868
3% CTAB-mont-PU	4.76	1.931
5% CTAB-mont-PU	4.42	2.055
1% ODA-mont-PU	4.48	2.040
3% ODA-mont-PU	2.62	3.386
5% ODA-monr-PU	2.42	3.607

The improved dispersion observed in CTAB- and especially ODA-modified montmorillonite originates from the surfactant modification process. The ion-exchange of Na^+ with long-chain organic cations increases the hydrophobicity of the clay surface and reduces its surface energy. This modification expands the interlayer spacing (as confirmed by the WAXD results), making it easier for polyurethane chains to penetrate between the silicate layers. The presence of long alkyl chains also enhances compatibility with the non-polar soft segments of palm-oil-based PU, facilitating polymer–clay interactions and promoting intercalation and partial exfoliation. As a result, surfactant-modified clays disperse more uniformly in the PU matrix compared to unmodified clay.

3.3.2 FTIR spectra

FTIR analysis (Figures 11 and 12) showed identical characteristic peaks for pure PU and PU/clay nanocomposites, indicating that the polyurethane structure remained unchanged and no significant interactions occurred between organoclay layers and PU molecules.

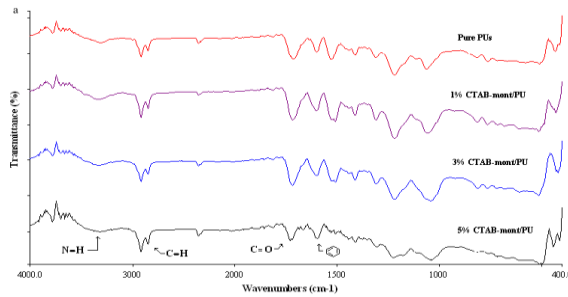

Figure 11: The FTIR spectra of pure PU and 1,3,5% CTAB-mont-PU.

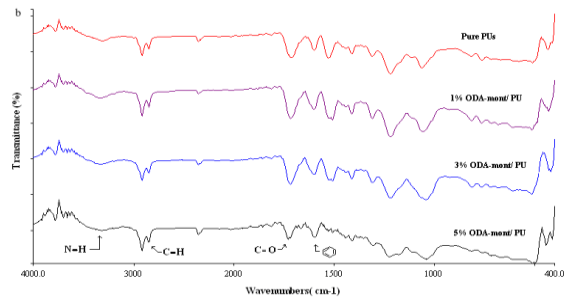

Figure 12: The FTIR spectra of pure PU and 1,3,5% ODA-mont-PU.

The influence of intercalated silicate layers on the phase separation of polyurethane can be assessed through the hydrogen bonding behavior within the hard segments. FTIR shows peaks at 3320 cm^{-1} (hydrogen-bonded –NH) and 3480 cm^{-1} (free –NH) [24]. –NH groups act as proton donors, bonding with carbonyl oxygens in hard segments and ether oxygens in soft segments. Urethane carbonyl peaks appear at 1733 cm^{-1} (free) and 1703 cm^{-1} (hydrogen-bonded) [25]. Assignments of these bands are summarized in Table 2 [26].

Table 2: Assignments of the absorption bands in FT-IR spectra of polyurethane.

Freq. (cm^{-1})	Assignment	Domain Origin
3480	ν(NH), free	hard segment
3320	ν(NH), hydrogen-bonded	hard segment
3320	ν(CH_2), free	soft segment
2935	ν(C=O), free urethane carbonyl	hard segment
1733	ν(C=O), Hydrogen bondeds	hard segment

Table 3 shows DPS and DPM values of PU and PU/organoclay nanocomposites. Pure PU had a phase separation ratio of ~52%, and the addition of CTAB- or ODA-mont caused almost no change, regardless of clay content. This indicates uniform nanometer-scale dispersion of silicate layers in the PU matrix, consistent with earlier reports [27], [28].

Table 3: Absorption of carbonyl and degree of phase separation.

Materials	$\frac{A_{1709}}{A_{1731}}$	DPS (%)	DPM (%)
Pure PU	0.9288	48.10	51.90
1% CTAB-mont-PU	0.9625	49.04	50.95
3% CTAB-mont-PU	0.9287	48.15	51.85
5% CTAB-mont-PU	0.9623	49.03	50.97
1% ODA-mont-PU	0.9637	49.07	50.93
3% ODA-mont-PU	0.9612	49.01	50.99
5% ODA-monr-PU	0.9617	49.02	50.98

3.3.3 Molecular weight (MW)

The molecular weights (MW) of pure PU and PU/clay nanocomposites are summarized in Table 4. Pure PU exhibited an MW of 3915.19, which increased with the incorporation of modified clays. For CTAB–mont–PU, the MW values were 4160.33, 4360.29, and 4417.25 at 1%, 3%, and 5% loading, respectively. Similarly, ODA–mont–PU showed MW values of 4245.12, 4429.45, and 4610.11 for 1%, 3%, and 5% concentrations, indicating that higher organoclay content led to an increase in molecular weight.

In each case, corresponding to the fact that the segmented PU structures were affected by the presence of organoclay as identified by their FTIR spectra, the molecular weight of pure PU and PU/ clay nanocomposites in general was not strongly affected by the addition of organoclay; this result is similar to the research by [29].

3.3.4 Mechanical properties

Table 4 and Figures 11 show that the incorporation of organoclay notably enhanced the tensile strength and elongation at break of the PU nanocomposites, with both parameters increasing proportionally to the clay content. The ODA-modified samples exhibited the highest performance values. The rise in elongation indicates strong interactions between PU and treated clays [30].

The improvement in tensile modulus can also be attributed partly to the formulation parameters. The use of a slightly excess NCO/OH ratio (1.05) increases the effective crosslink density of the polyurethane matrix, which contributes to higher stiffness and enhanced tensile properties.

Table 4: Number-average molecular weight and mechanical properties of pure PU and PU/clay nanocomposites.

Materials	MW	Tensile Strength (Mpa)	Elongation at break
Pure PU	3266.19	14.983	253.4
1% CTAB-mont-PU	3960.33	21.766	270.7
3% CTAB-mont-PU	3809.29	28.342	415.3
5% CTAB-mont-PU	3917.25	32.178	431.1
1% ODA-mont-PU	3745.12	30.491	490.0
3% ODA-mont-PU	3929.45	39.257	677.9
5% ODA-mont-PU	3810.11	40.100	700.5

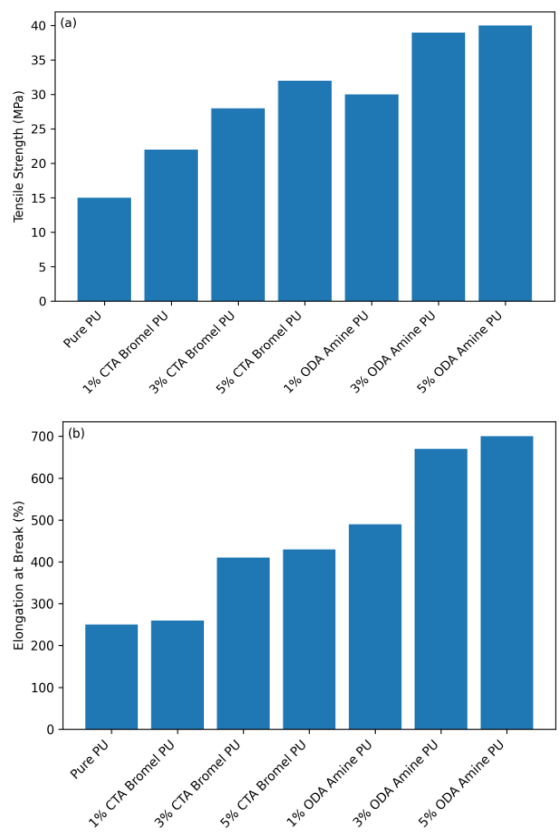

Figure 13: (a) Tensile strength of pure PU and PU/clay nanocomposites (b) Elongation at break of pure PU and PU/clay nanocomposites.

Table 4 and Figures 13 show that adding 5 wt% clay enhanced tensile strength by over 214% (CTAB-mont) and 268% (ODA-mont), with elongation at break also improving, indicating strong PU–clay

interactions [31]. ODA-mont provided superior reinforcement, making it more effective for elastomer applications requiring higher modulus, hardness, and tear strength.

The superior reinforcement of ODA-modified montmorillonite compared to CTAB-modified clay can be explained by the interfacial mechanism between the surfactant-modified silicate layers and the PU matrix. ODA contains a longer non-polar C18 alkyl chain, which exhibits higher hydrophobic compatibility with the soft segment of palm-oil-based PU that is inherently lipophilic. This compatibility reduces interfacial surface energy and enables stronger physical interactions, promoting more effective adhesion between polymer chains and the clay surface.

In contrast, CTAB contains a shorter C16 alkyl chain and a quaternary ammonium head group, which introduces ionic character that is less compatible with the predominantly non-polar PU soft segments. As a result, CTAB-modified clay shows weaker interfacial adhesion and less efficient stress transfer.

The increased hydrophobic matching of ODA also stabilizes the intercalated/exfoliated morphology, as observed in XRD and TEM data, leading to more uniform platelet dispersion. This morphology facilitates better confinement of polymer chains and enhances stress transfer during deformation. Consequently, ODA–mont–PU exhibits higher tensile strength, elongation at break, and thermal stability compared to CTAB–mont–PU.

3.3.5 Modeling Young's Modulus of Polyurethane/Clay nanocomposites

The mechanical behavior of PU/clay nanocomposites, particularly the Young's modulus, was modeled using the Guth, Halpin–Tsai, and modified Halpin–Tsai equations. Experimental measurements at different clay loadings (Table 5) were compared with model predictions to evaluate reinforcement effects.

Table 5: Measured tensile modulus (E) of PU/clay nanocomposites.

Materials	Wt % clay	Tensile modulus (MPa)
Pure PU	0	118.694
1% CTAB-mont-PU	1	127.252
3% CTAB-mont-PU	3	130.688
5% CTAB-mont-PU	5	140.575
1% ODA-mont-PU	1	130.798
3% ODA-mont-PU	3	132.781
5% ODA-mont-PU	5	144.550

Figure 14 The results indicate that the experimental modulus values of 1–5 wt% CTAB–mont–PU and ODA–mont–PU nanocomposites were in good agreement with the Guth model predictions, whereas the Halpin–Tsai equation accurately described the behavior only at low clay contents (<1 wt%).

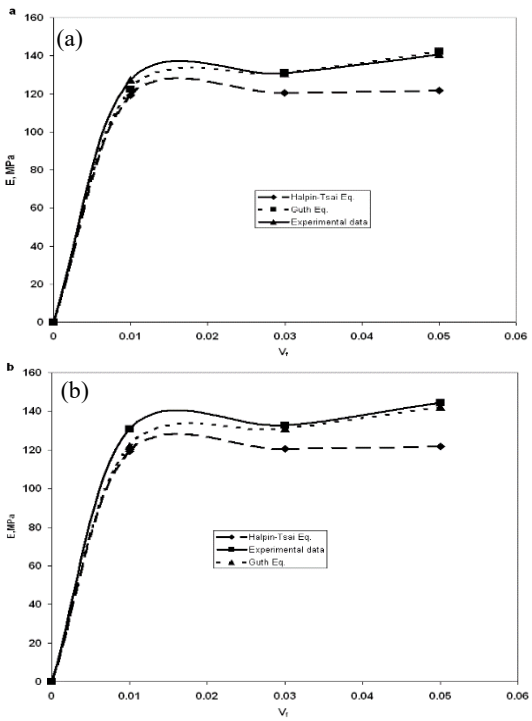

Figure 14: Comparison between experimental modulus and theoretical predictions using Guth and Halpin–Tsai models for (a) CTAB–mont–PU and (b) ODA–mont–PU.

The Halpin–Tsai model suggests that composite performance is governed by the volume fraction and aspect ratio of the reinforcing phase. In PU/clay nanocomposites, exfoliated clay platelets (~1 nm thick, 500–2000 nm wide) reinforced the matrix, as confirmed by XRD [32]. Young's modulus increased with clay loading, reaching 144.55 MPa at 5% ODA-mont-PU due to strong interfacial interactions and hydrogen bonding, with ODA-mont showing superior performance over CTAB-mont. DMA (Figures 15) further revealed higher Tg values in nanocomposites than in pure PU (–12.2 °C), rising to –6.8 °C (CTAB-mont) and –5.0 °C (ODA-mont) at 5% loading, reflecting stronger confinement and hydrogen bonding [33], [34].

The tan δ curves shown in Figure 15 reveal that the glass transition temperature (Tg) of the polyurethane matrix increases progressively with the incorporation of CTAB-montmorillonite and ODA-montmorillonite clays. The shift of the tan δ peak toward higher temperatures indicates reduced molecular mobility within the soft segment domains. This behavior is consistent with the confinement effect produced by the dispersed clay platelets and the formation of additional hydrogen bonding interactions between urethane groups and the organoclay surfaces. To clarify this observation, the Tg values obtained from tan δ peak positions are summarized in Table 6.

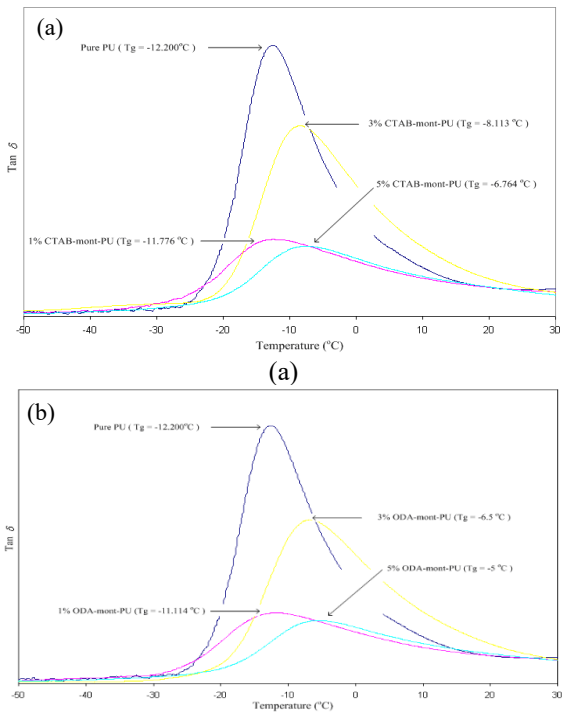

Figure 15: (a) DMA curves for tan δ of pure PU and CTAB-mont-PU 1, 3, 5 wt% (b) DMA curves for tan δ of pure PU and ODA-mont-PU 1, 3, 5 wt%.

Table 6: Glass transition temperature (Tg) obtained from tan δ peak of PU and PU/organoclay nanocomposites.

Sample	Tg (°C)
Pure PU	–12.2
1% CTAB-mont-PU	–10.5
3% CTAB-mont-PU	–8.7
5% CTAB-mont-PU	–6.8
1% ODA-mont-PU	–9.8
3% ODA-mont-PU	–6.2
5% ODA-mont-PU	–5.0

3.3.6 Thermal stability

The thermal degradation behavior of pure PU and its nanocomposites was investigated using TGA, as illustrated in Figures 16(a) and (b). Pure PU followed a typical three-stage degradation profile, with an initial weight loss starting at approximately 200 °C and completing near 700 °C, corresponding to the labilization of urethane bonds. In contrast, the incorporation of modified montmorillonite (MMT) significantly enhanced the thermal resistance, shifting the major decomposition stages to higher temperatures. PU/clay nanocomposites exhibited much higher thermal resistance, with onset at ~318 °C (CTAB-mont-PU) and ~330 °C (ODA-mont-PU), giving over 62% improvement, where ODA-mont-PU provided the best stability.

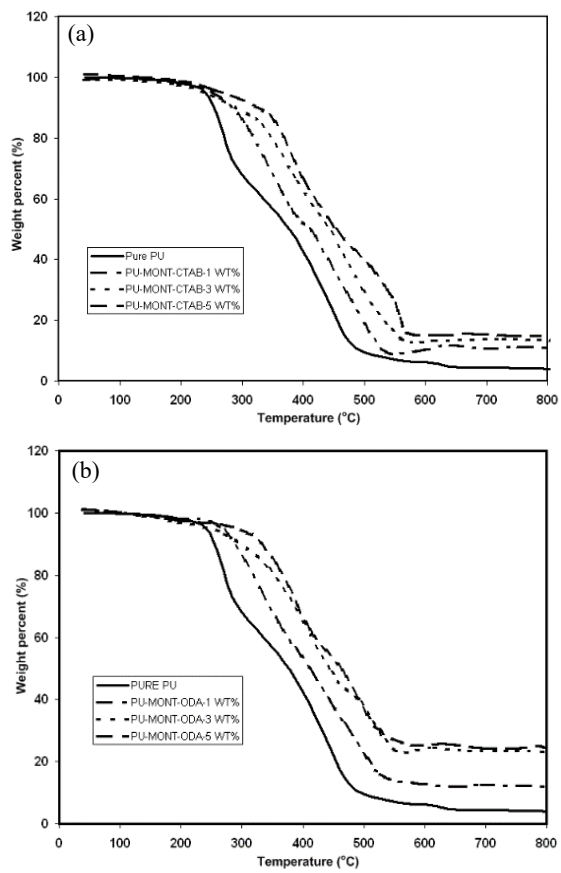

Figure 16: (a) TGA curves of pure PU and PU/clay nanocomposites with 1, 3, and 5 wt% CTAB–mont–PU; (b) TGA curves of pure PU and PU/clay nanocomposites with 1, 3, and 5 wt% ODA–mont–PU.

Between 100–275 °C, PU/clay nanocomposites degraded slightly faster than pure PU due to early decomposition of CTAB and ODA molecules at low loadings (1–3 wt%). After their decomposition, the composites showed higher thermal resistance above 400 °C, as clay layers restricted heat transfer and slowed further degradation. Among the formulations, the ODA-modified MMT provided the highest stability. This is consistent with the WAXD results, where ODA demonstrated a larger d-spacing than CTAB. The greater interlayer expansion and longer alkyl chains of ODA likely facilitate better exfoliation of the clay layers, creating a more robust interfacial interaction with the PU matrix and a more effective barrier against thermal energy.

The improvement in thermal stability of the nanocomposites is primarily attributed to the barrier effect created by the clay layers. The dispersed silicate platelets reduce the diffusion rate of heat, oxygen, and volatile degradation products, thereby delaying the onset of thermal decomposition. Additionally, the restricted mobility of polymer chains due to interfacial interactions increases the activation energy required for bond scission. During thermal degradation, nanoclay also promotes the formation of a protective char layer that acts as an insulating barrier, further enhancing high-temperature stability. These mechanisms collectively account for the increase in onset degradation temperature and higher thermal resistance in PU/clay nanocomposites.

3.3.7 Thermal degradation kinetics of PU/Clay nanocomposites

A pseudo–first-order kinetic model was applied to TGA data (Figures 17–23). Plots of Ln[–(dw/dt)/w] vs –1/T gave activation energy (E) and frequency factor (A), summarized in Table 7. Results show that organoclay, particularly at 5 wt% CTAB-mont-PU and ODA-mont-PU, markedly increased activation energy, indicating reduced molecular mobility and improved thermal stability [35].

Table 7: Kinetic parameters obtained by linear regression analysis.

Materials	E (kJ/mol)	Ln A (min^{-1})
Pure PU	187.150	7.1333
1% CTAB-mont-PU	1437.657	3.0050
3% CTAB-mont-PU	1563.448	2.4726
5% CTAB-mont-PU	1863.001	1.6555
1% ODA-mont-PU	1528.695	2.6075
3% ODA-mont-PU	1585.230	1.2755
5% ODA-mont-PU	1960.026	1.0434

The data indicate that PU/clay nanocomposites have higher energy barriers for chain motion than pure PU, resulting in lower molecular mobility. Reduced mobility limits the transport of reactive species, giving the nanocomposites greater chemical and thermal stability [36].

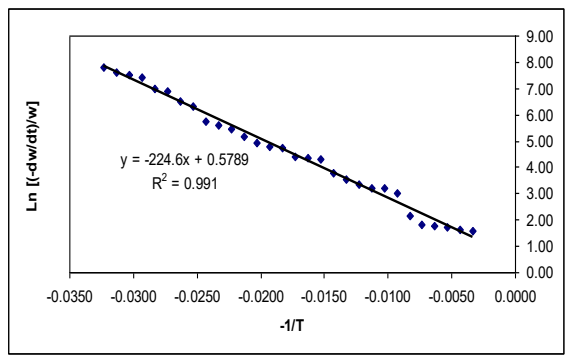

Figure 17: First-order kinetic plot of pure Polyurethane.

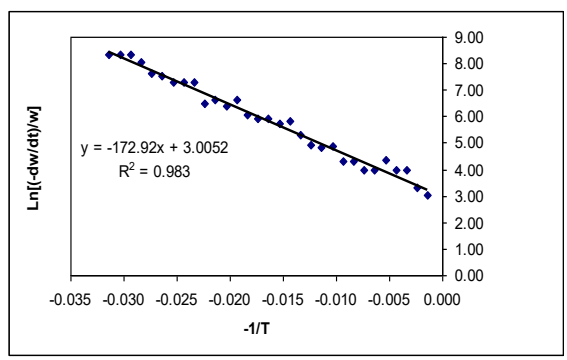

Figure 18: First-order kinetic plot of PU/Clay nanocomposites CTAB 1 wt%.

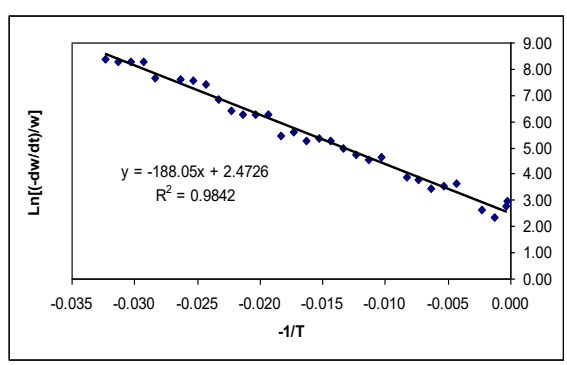

Figure 19: First-order kinetic plot of PU/Clay nanocomposites CTAB 3 wt%.

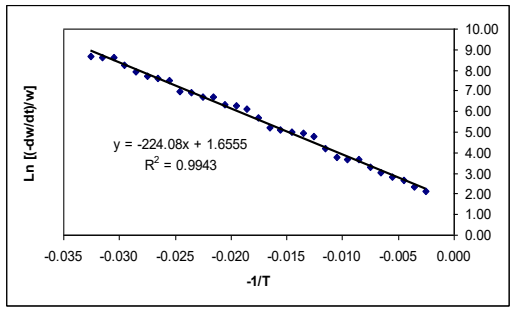

Figure 20: First-order kinetic plot of PU/Clay nanocomposites CTAB 5 wt%.

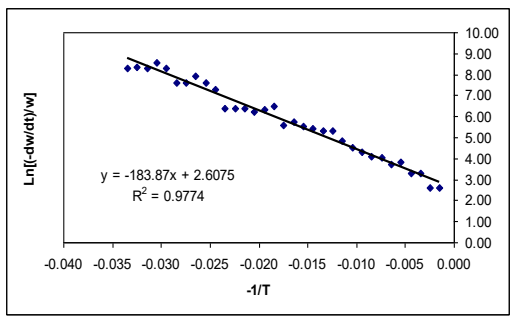

Figure 21: First-order kinetic plot of PU/Clay nanocomposites ODA 1 wt%.

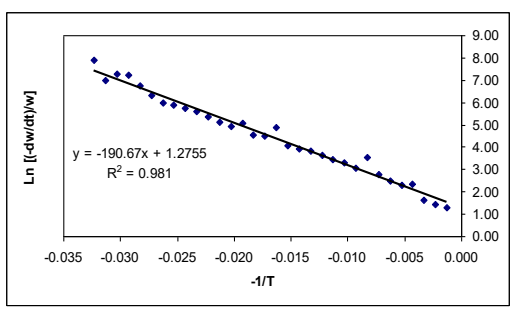

Figure 22: First-order kinetic plot of PU/Clay nanocomposites ODA 3 wt%.

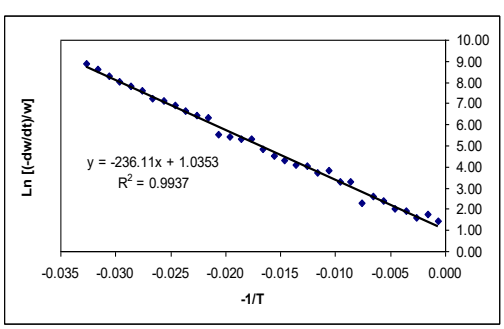

Figure 23: First-order kinetic plot of PU/Clay nanocomposites ODA 5 wt%.

3.3.8 Scanning Electron Microscopy (SEM)

SEM images (Figure 24) show fractured surfaces of PU and PU/clay nanocomposites. Fillers were coated and surface-treated to enhance bonding with the PU matrix. The observations revealed the formation of an interphase region, rather than a sharp interface, due to physical mixing and chemisorption at the filler surface [37].

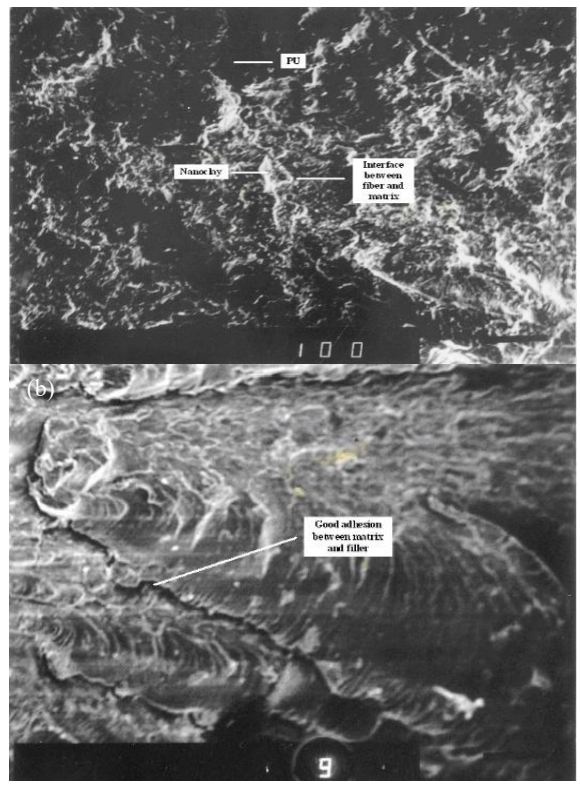

Figure 24: (a) SEM micrographs of interfacial adhesion between nanoclay and matrix PU (b) SEM micrographs of a good dispersion between nanoclay and ODA-Mont- PU 3 wt%.

Composite effectiveness depends on fiber–matrix cooperation through the interface, which transfers stress and governs mechanical properties. The matrix transfers load to fibers via interfacial shear stress, requiring strong bonding [38] (Figure 24 (a)). SEM (Figure 24 (b)) shows that 3 wt% ODA-Mont-PU achieves good dispersion, which reported finer nanoclay dispersion in polymer matrices due to alkylammonium treatment, though small aggregates remain visible.

3.3.9 Transmission Electron Microscope (TEM)

TEM (Figures 25–30) showed that PU/clay nanocomposites contained silicate layers reduced to the nanometer scale, intercalated or exfoliated in the matrix, with some stacked domains remaining [39]. At 1 wt% clay, complete intercalation was observed, while higher loadings produced mixed intercalated–exfoliated structures with fine distributions. Strong polymer–clay interactions and increased viscosity during shear mixing promoted delamination, polymer chain intercalation, and expanded basal spacing [40].

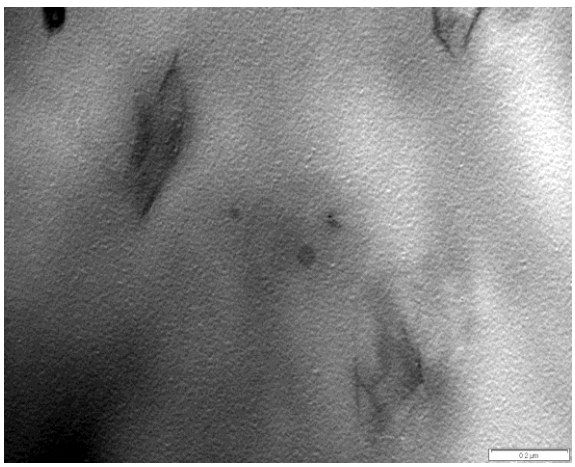

Figure 25: TEM image of PU/clay nanocomposite containing 1 wt% CTAB–mont.

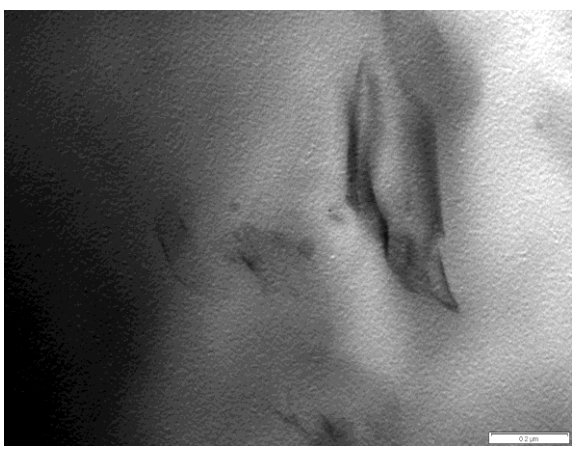

Figure 26: TEM image of PU/clay nanocomposite containing 1 wt% ODA–mont.

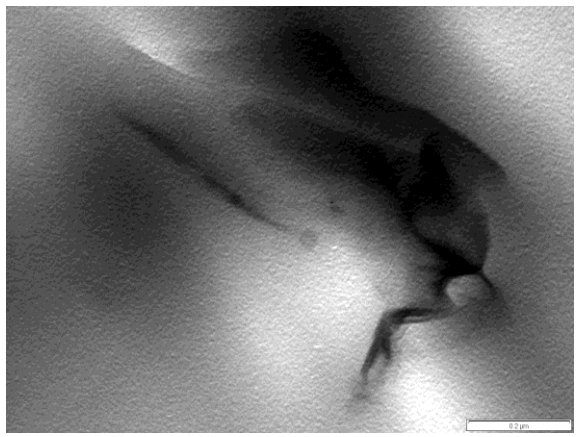

Figure 27: TEM image of PU/clay nanocomposite containing 3 wt% CTAB–mont.

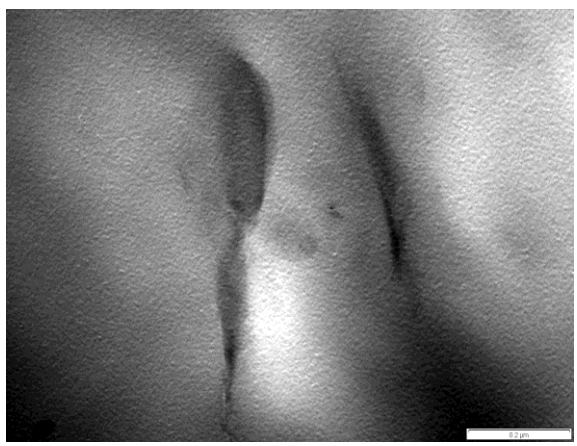

Figure 28: TEM image of PU/clay nanocomposite containing 3 wt% ODA–mont.

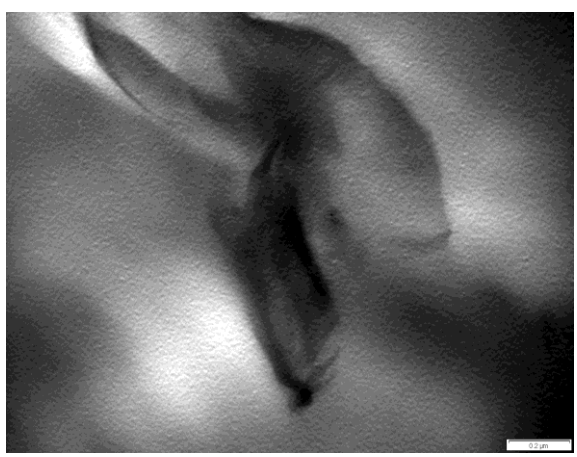

Figure 29: TEM image of PU/clay nanocomposite containing 5 wt% CTAB–mont.

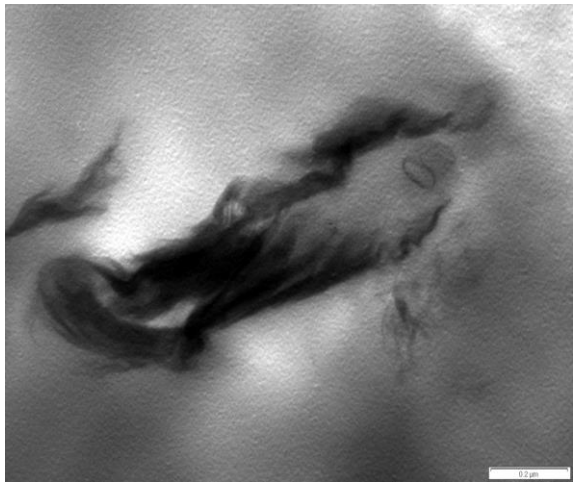

Figure 30: TEM image of PU/clay nanocomposite containing 5 wt% ODA–mont.

The TEM observations are fully consistent with the XRD results. The increase in d-spacing up to 3.6 nm at 5 wt% loading (as shown in the WAXD analysis) confirms a well-intercalated structure, accompanied by localized regions of partial exfoliation. TEM micrographs show a relatively uniform and isolated distribution of clay platelets at 5 wt%, with no evidence of significant reaggregation. This indicates that the interfacial interactions between the polyurethane matrix and the surfactant-modified clays were sufficiently strong to prevent restacking. Reaggregation typically occurs only at much higher clay concentrations or when the polymer–clay compatibility is poor, which was not observed in this system.

It is well recognized that nanoparticle/nanofiller reinforcement can exhibit a dose-dependent limitation, where increasing filler content may promote particle–particle interactions and agglomeration, thereby reducing the expected performance gains. In the present PU/organoclay system, this potential drawback was mitigated through surfactant modification of montmorillonite (CTAB and ODA), which expanded the basal spacing and improved polymer–clay compatibility, facilitating intercalation/exfoliation rather than restacking. Consistent evidence from WAXD/XRD, SEM, and TEM confirms that the organoclays remained well-dispersed up to 5 wt% loading, with expanded interlayer spacing (up to ~3.6 nm) and no pronounced reaggregation observed at this composition. These observations indicate that the interfacial interactions between the polyurethane matrix and the organoclay surfaces were sufficiently strong to suppress agglomeration within the investigated loading range.

4 Conclusions

High molecular weight polyurethane (PU) elastomers were successfully synthesized from palm oil-based polyols obtained by esterification of oleic acid and glycerol using DBSA as both catalyst and emulsifier. The formation of polyols and PUs was confirmed by FTIR, while GPC analysis indicated molecular weights of ~950 for polyol and ~3266 for PU, confirming high polymer formation. To improve the properties of PU, montmorillonite (MMT) clays were modified with CTAB and ODA surfactants, producing organoclays with expanded d-spacings of 1.571 nm and 1.798 nm compared to 1.142 nm for pure MMT, indicating successful intercalation. WAXD, SEM, and TEM analyses revealed fine dispersion of clay platelets and effective intercalated–exfoliated structures in the PU matrix.

Mechanical tests showed that the tensile strength and elongation at break improved by over 200% with organoclay addition, highlighting strong interfacial interactions between PU and clay. DMA confirmed an increase in glass transition temperature (Tg), attributed to confinement effects and hydrogen bonding between urethane groups and clay surfaces. Thermal stability was also enhanced, as TGA showed that the onset of degradation shifted from 200 °C for pure PU to ~318 °C for CTAB-mont-PU and ~330 °C for ODA-mont-PU, representing more than 62% improvement. Overall, ODA-mont-PU exhibited superior reinforcement compa330 red to CTAB-mont-PU, providing better morphology, mechanical performance, and thermal resistance, making it highly promising for advanced elastomer applications.

While the use of palm-oil-based polyols contributes to renewable feedstock utilization, the specific environmental impacts cannot be quantified without conducting a full Life Cycle Assessment (LCA). Therefore, future studies should include LCA analysis to rigorously validate the sustainability claims.

Future work should include comprehensive DMA storage modulus (E') measurements to further verify the confinement effect and polymer chain mobility reduction suggested by the observed Tg shift.

Acknowledgments

The author would like to express his gratitude and high appreciation to the Ministry of Higher Education, Science and Technology, Directorate General of Research and Development, and the Lhokseumawe State Polytechnic, which provided funding through grant number 037/C3/DT.05.00/PL/ 2025.

Author Contributions

T.R.: conceptualization and supervision, methodology and validation, S.: data collection and experimentation, data curation and formal analysis, P.N.A. and M.Y.: methodology and editing, resources and project administration, F.S.: draft writing and data processing, review and reference compilation. All authors have read and approved the final version of the manuscript.

Conflicts of Interest

The authors declare no conflict of interest.

Declaration of generative AI and AI-assisted technologies in the writing process

The authors utilized the ChatGPT tool to enhance the language and readability of the manuscript.

References

[1] T. Rihayat *et al.,* "Mechanical characterisation of polyurethane/clay nanocomposites," *Polymers and Polymer Composites*, vol. 15, no. 8, pp. 647–652, 2007, doi: 10.1177/096739110701500808.

[2] R. Ridwan, T. Rihayat, S. Suryani, A. S. Ismi, N. Nurhanifa, and S. Riskina, "Combination of poly lactid acid zinc oxide nanocomposite for antimicrobial packaging application," *IOP Conference Series: Materials Science and Engineering*, vol. 830, no. 4, 2020, doi: 10.1088/1757-899X/830/4/042018.

[3] Suryani, H. Agusnar, B. Wirjosentono, T. Rihayat, and Nurhanifa, "Improving the quality of biopolymer (poly lactic acid) with the addition of bentonite as filler," *IOP Conference Series: Materials Science and Engineering*, vol. 222, no. 1, 2017, doi: 10.1088/1757-899X/222/1/012008.

[4] Wang *et al.,* "Soft-hard hybrid covalent-network polymer sponges with super resilience, recoverable energy dissipation and fatigue resistance under large deformation," *Materials Science and Engineering: C*, vol. 126, 2021, Art. no. 112185, doi: 10.1016/J.MSEC.2021.112185.

[5] J. Palanivel, J. Srinivasan, and N. C. S. Chakravathy, "Comparison of the frictional resistance and optical properties of aluminum oxide and zinc oxide coated nickel titanium archwires – An *in vitro* study," *APOS Trends in Orthodontics*, vol. 12, no. 3, pp. 168–175, 2022, doi: 10.25259/APOS_24_2022.

[6] Kanagaraj, G. Sekar, T. Arokiyasamy, D. Arumugam, and S. Ramakrishnan, "Synthesis of rigid polyurethane foams with palm oil based flame retardant polyols," *International Journal of Progressive Research in Engineering Management and Science*, vol. 3, no. 7, pp. 449–459, 2023, doi: 10.58257/ijprems31848.

[7] V. Tencau, and E. P. Kurniasih, "Determinan ekspor crude palm oil (cpo) indonesia, malaysia dan thailand," *Kindai: Jurnal Manajemen Dan Akuntansi*, vol. 20, no. 3, pp 285–302, 2024, doi: 10.35972/kindai.v20i3.1793.

[8] K. Y. Sen, and S. Baidurah, "Renewable biomass feedstocks for production of sustainable biodegradable polymer," *Green and Sustainable Chemistry*, vol. 27, 2021, Art. no. 100412, doi: 10.1016/J.COGSC.2020.100412.

[9] W. Senusi *et al.,* "Comparative assessment for biodiesel production from low-cost feedstocks of third oil generation," *Renewable Energy*, vol. 236, pp. 121369, 2024, doi: 10.1016/j.renene. 2024.121369.

[10] K. Cheng, and Z. Heidari, "A new method for quantifying cation exchange capacity in clay minerals," *Applied Clay Science*, vol. 161, pp. 444–455, 2018, doi: 10.1016/J.CLAY.2018. 05.006.

[11] R. Mazurenko *et al.,* "Polymer nanocomposites based on nanosized substituted ferrites (NiZn)1−xMnxFe_2O_4 on the surface of carbon nanotubes for effective interaction with high-frequency EM radiation," *Materials*, vol. 17, no. 5, p. 986, 2024, doi:10.3390/ma17050986.

[12] S. Skupiński, M. Kalbarczyk, D. M. Kamiński, and M. Kosmulski, "Surface chemistry aspects of ion exchange in basic copper salts," *Molecules*, vol. 30, no. 1, pp. 21, 2024, doi: 10. 3390/molecules30010021.

[13] P. Gready, "First encounters: Early career researchers and fieldwork," *Journal of Human Rights Practice*, vol. 6, no. 2, pp. 195–200, 2014, doi: 10.1093/jhuman/huu013.

[14] Z. He et al., "In situ synthesis of polymer-modified boron nitride nanosheets via anionic polymerization," *Applied Surface Science*, vol. 537, 2021, Art. no. 147966, doi: 10.1016/j.apsusc.2020.147966.

[15] C. Salgado, M. P. Arrieta, L. Peponi, M. Fernández-García, and D. López, "Silica-nanocomposites of photo-crosslinkable poly(urethane)s based on poly(ε-caprolactone) and coumarin," *European Polymer Journal*, vol. 93, pp. 21–32, 2017, doi: 10.1016/j.eurpolymj. 2017.05.030.

[16] H. L. Su *et al.,* "An efficient Zr-ZSM-5-st solid acid catalyst for the polyol esterification reaction," *Catalysts*, vol. 12, no. 8, p. 901, 2022, doi: 10.3390/catal12080901.

[17] C. Uhl *et al.,* "Long-term results of the heparin-bonded Viabahn stent graft in femoropopliteal TASC C and D lesions with a covered stent length of minimum 25 cm," *Vascular*, vol. 27, no. 5, pp. 553–559, 2019, doi: 10.1177/170853 8119840863.

[18] H. T. Zhang, F. Zhang, and Y. X. Wu, "Robust stretchable thermoplastic polyurethanes with long soft segments and steric semisymmetric hard segments," *Industrial & Engineering Chemistry Research*, vol. 59, no. 10, pp. 4483–4492, 2020, doi: 10.1021/acs.iecr.9B06107.

[19] P. Kasprzyk, H. Beneš, R. K. Donato, and J. Datta, "The role of hydrogen bonding on tuning hard-soft segments in bio-based thermoplastic poly(ether-urethane)s," *Journal of Cleaner Production*, vol. 274, pp. 122678, 2020, doi: 10.1016/j.jclepro.2020.122678.

[20] K. Fujii, T. Mukai, and K. Nishikawa, "Crystal structure of 1,3-Dimethylimidazolium Bis(fluorosulfonyl)amide: Unexpectedly high melting point arising from polydentate hydrogen bonding," *Chemistry Letters*, vol. 43, no. 4, pp. 405–407, 2014, doi: 10.1246/cl.130982.

[21] J. Yu, W. Zhou, and G. Zhao, "Influence of strain, temperature, and strain rate on interfacial structure and strength of AZ31BMg/6063Al formed by plastic deformation bonding," *Journal of Manufacturing Processes*, vol. 65, pp. 299–311, 2021 doi: 10.1016/j.jmapro.2021.03.026.

[22] N. A. Selamat, M. N. M. Ansari, Z. Yahya, and R. E. Naicker, "Mechanical properties of polypropylene (PP) - Montmorillonite (MMT) nanocomposites for pre-fabricated vertical drain (PVD) application," *International Journal of Engineering and Technology*, vol. 7, no. 4, pp. 689–692, 2018, doi: 10.14419/ijet.v7i4.35.23090.

[23] A. F. Qadikolae and S. Sharma, "Facet selectivity of cetyltrimethyl ammonium bromide surfactants on gold nanoparticles studied using molecular simulations," *Journal of Physical Chemistry B*, vol. 126, no. 48, pp. 10249–10255, 2022, doi: 10.1021/acs.jpcb.2c06236.

[24] J. M. Young *et al.,*, "Nano-FTIR investigation of the CM Chondrite Allan Hills 83100," *Journal Of Geophysical Research: Planets*, vol. 127, no. 5, 2022, doi: 10.1029/2021 je007166.

[25] M. Lee, B. E. Cohen, A. J. Boyce, L. J. Hallis, and L. Daly, "The pre-atmospheric hydrogen inventory of CM carbonaceous chondrites," *Geochimica et Cosmochimica Acta*, vol. 309, pp. 31–44, 2021, doi: 10.1016/j.gca.2021.06.013.

[26] V. D'Anna, A. Spyratou, M. Sharma, and H. Hagemann, "FT-IR spectra of inorganic borohydrides," *Spectrochimica Acta Part A: Molecular and Biomolecular Spectroscopy*, vol. 128, pp. 902–906, 2014 doi: 10.1016/j.saa.2014. 02.130.

[27] B. D. Partain *et al.,* "Spatially-resolved nanometer-scale measurement of cartilage extracellular matrix mobility," *Osteoarthritis and Cartilage*, vol. 29 no. 9, pp. 1351–1361, 2021, doi: 10.1016/j.joca.2021.05.059.

[28] Q. Yao, J. W. Park, C. Won, S. Cheong, and H. W. Yeom, "Nanometer-scale 1D negative differential resistance channels in van der waals layers," *Advanced Science*, 2024, doi: 10.1002/ advs.202408090.

[29] G. Dias *et al.,* "Hybrid Pu/synthetic Talc/organic clay ternary nanocomposites: Thermal, mechanical and morphological properties," *Polymers & Polymer Composites*, vol. 26, no. 2, pp. 127–140, 2018, doi: 10.1177/096739111 802600201.

[30] V. Belitsky and G. M. Schütz, "RNA Polymerase interactions and elongation rate," *Journal of Theoretical Biology*, vol. 462, pp. 370–380, 2019, doi: 10.1016/J.JTBI.2018.11.025.

[31] M. Breckheimer, S. Amayri, D. Ferreira Sánchez, D. Grolimund, and T. Reich,

"Geochemical interactions of Np and Pu with pyrite heterogeneities in Opalinus Clay in the context of deep geological repositories," *EGU General*, 2024, doi: 10.5194/egusphere-egu24-21650.

[32] Y. Zare, "A model for tensile strength of polymer/clay nanocomposites assuming complete and incomplete interfacial adhesion between the polymer matrix and nanoparticles by the average normal stress in clay platelets," *RSC Advances*, vol. 6, no. 63, pp. 57969–57976, 2016, doi: 10.1039/C6RA04132A.

[33] I. M. Rajkumar, D. Asaithambi, R. R. Chidambaram, and P. Rajkumar, "Double Schiff bases derivatives of chitosan by selective C-6 and C-2 oxidation mediated by 5-fluorosalicylaldehyde aniline by TG-GC-MS and TG-FTIR analysis," *Synthetic Communications*, vo. 50, no. 17, pp. 2617–2628, 2020, doi: 10.1080/00397911.2020.1780614.

[34] M. A. Bespyatov *et al.,* "Low-temperature heat capacity of $Ir(C_5H_7O_2)$ (C_8H_{12})," *The Journal of Chemical Thermodynamics*, vol. 99, pp. 70–74, 2016, doi: 10.1016/J.JCT.2016.03.044.

[35] I. Robin, T. Gräning, Y. Yang, Y. Katoh, and S. J. Zinkle, "Microstructure and thermal stability of a structurally graded tungsten and reduced activation ferritic/martensitic steel joint," *Journal of Materials Research and Technology*, vol. 30, pp. 3663–3674, 2024, doi: 10.1016/j.jmrt.2024.04.087.

[36] G. P. Srivastava and I. O. Thomas, "Tunable thermal transport characteristics of nanocomposites," *Nanomaterials*, vol. 10, no. 4, pp. 673, 2020, doi: 10.3390/nano10040673.

[37] T. Lai, Y. Chen, B. Fang, and J. Wang, "Decrease in adhesion force at silica-mica interface with short contact time due to dynamic formation process of liquid bridge revealed on an AFM," *Journal of Adhesion*, vol. 98, no. 10, pp. 1501–1519, 2021, doi: 10.1080/00218464.2021.1924154.

[38] F. R. Poblete and Y. Zhu, "Interfacial shear stress transfer at nanowire-polymer interfaces with van der Waals interactions and chemical bonding," *Journal of The Mechanics and Physics of Solids*, vol. 127, pp. 191–207, 2019, doi: 10.1016/j.jmps.2019.03.013.

[39] Y. Zare and K. Y. Rhee, "Multistep modeling of Young's modulus in polymer/clay nanocomposites assuming the intercalation/exfoliation of clay layers and the interphase between polymer matrix and nanoparticles," *Composites Part A-Applied Science and Manufacturing*, vol. 102, pp. 137–144, 2017, doi: 10.1016/j.compositesa.2017.08.004.

[40] S. Aharonovich and C. E. Diesendruck, "Single chain polymer nanoparticles as shear-resilient viscosity modifiers for lubricating oils," *Reactive & Functional Polymers*, vol. 131, pp. 237–242, 2018, doi: 10.1016/j.reactfunctpolym.2018.07.018.